ELECTRONIC SUPPORTING INFORMATION

Mesoporous, anisotropic nanostructures from bioinspired polymeric catecholamine neurotransmitters and their application as photoacoustic imaging agents

Zhenzhen Lu,[a,†] Shahinur Acter,[a,†] Boon Mian Teo,[a] Alexis I. Bishop,[b] Rico F. Tabor,*[a] and Mark Louis P. Vidallon*[a]

[a] School of Chemistry, Monash University, Clayton, VIC, 3800, Australia

[b] School of Physics and Astronomy, Monash University, Clayton, VIC, 3800, Australia

* Correspondence to: A/Prof. Rico F. Tabor (rico.tabor@monash.edu); School of Chemistry, Monash University, Clayton, VIC, 3800, Australia

* Correspondence to: Dr. Mark Louis P. Vidallon (mark.vidallon@monash.edu); School of Chemistry, Monash University, Clayton, VIC, 3800, Australia

[†] These authors contributed equally to this work.

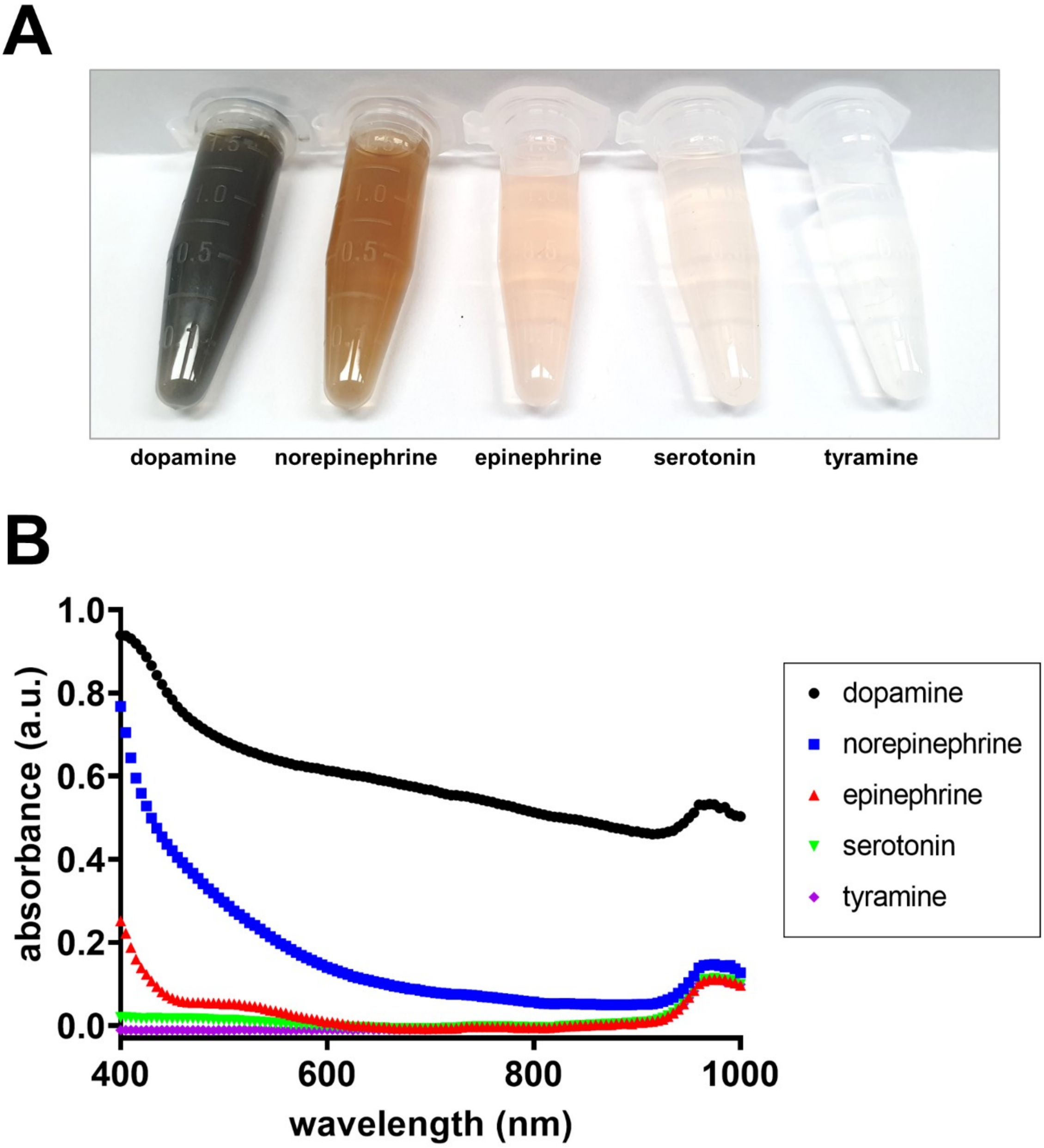

Figure S1. (**A**) Photograph showing the resulting mixtures from the polymerisation of various neurotransmitters and analogous molecules and (**B**) their respective absorbance spectra.

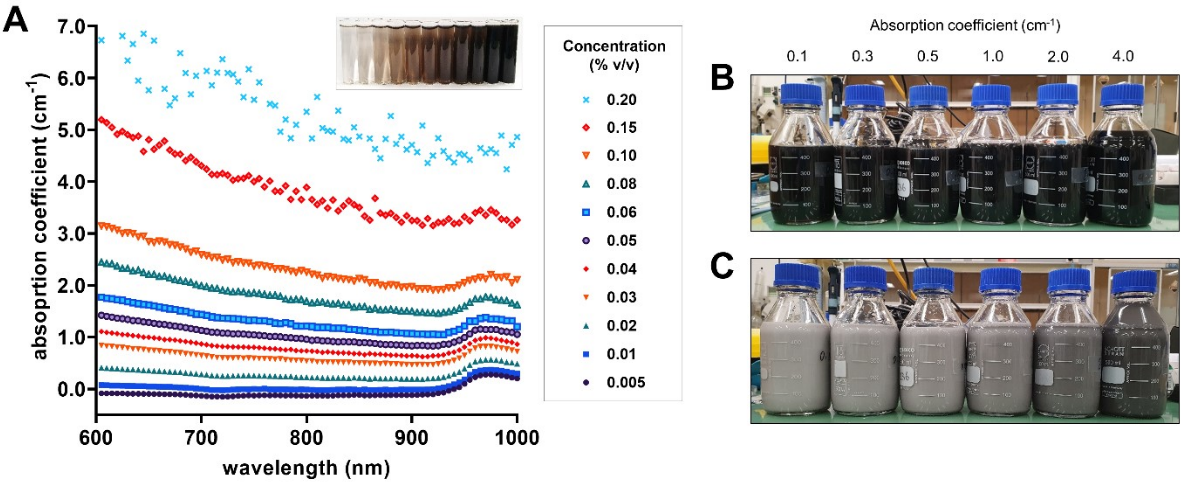

Figure S2. (**A**) Plot showing the experimental absorption coefficients of India ink at different volume concentrations as a function of wavelength. Inset shows a photograph of aqueous mixtures of India ink at different concentrations. Photographs showing (**B**) aqueous mixtures of India ink at different concentrations (0.017, 0.021, 0.026, 0.034, 0.055, 0.097, and 0.181% (v/v)) and (**C**) the resulting tissue mimicking phantoms after the addition of Intralipid® dispersion.

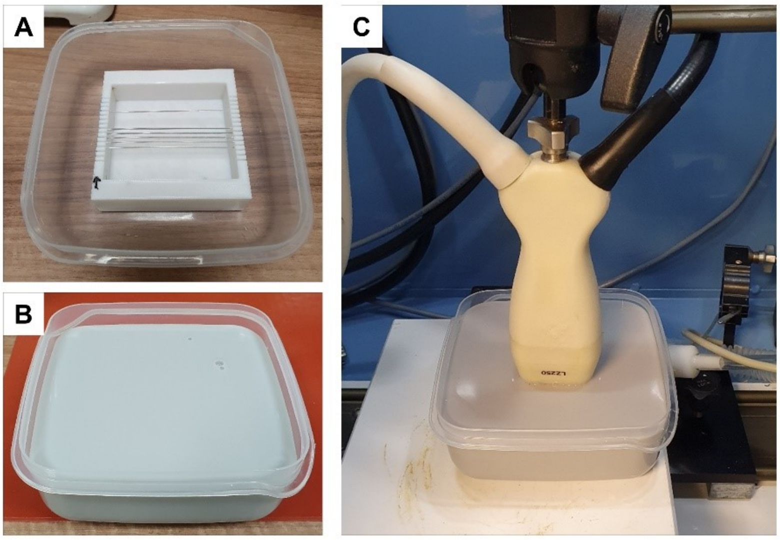

Figure S3. Photographs showing the polyethylene tubes with the samples, fixed onto the 3D-printed well (**A**) before and (**B**) after the addition of the external tissue-mimicking phantom, and (**C**) the final setup during photoacoustic imaging.

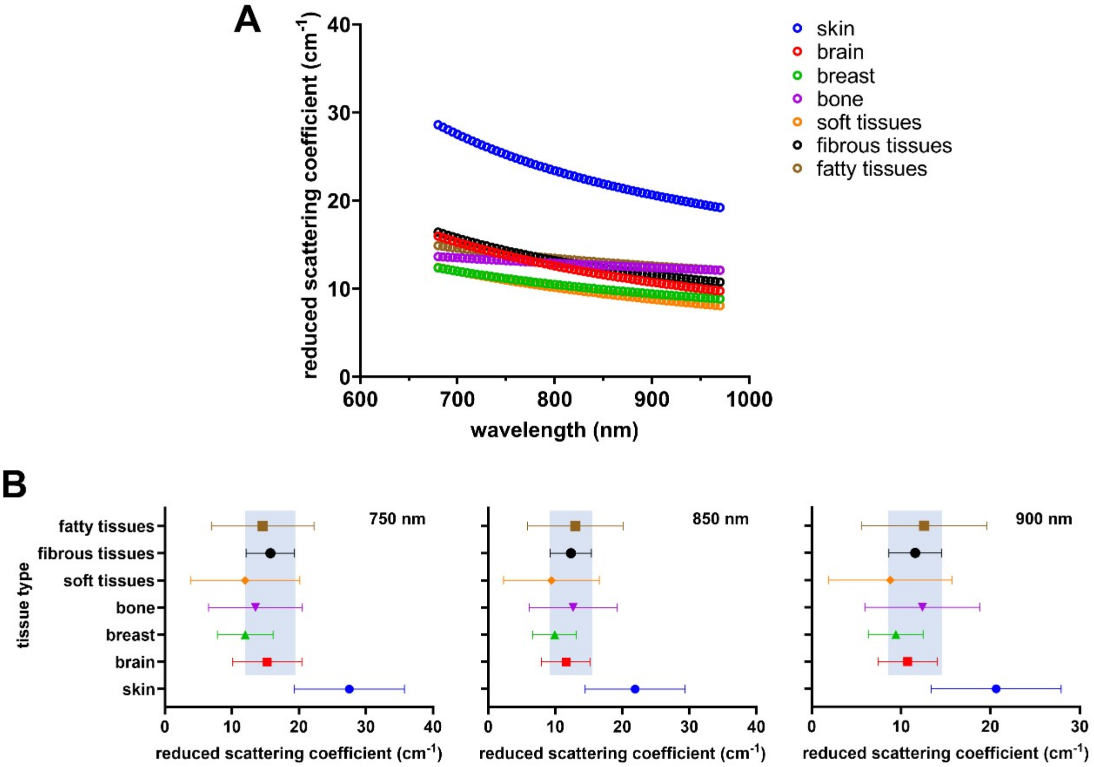

Figure S4. (**A**) Plot showing the mean reduced scattering coefficients of various biological tissues at different wavelengths, calculated based on parameters presented in the work of Jacques [1]. Plots in (**B**) shows the reduced scattering coefficients of various biological tissues at three different wavelengths, that are close to the peaks in the photoacoustic spectra of PDA, PNE, and PE.

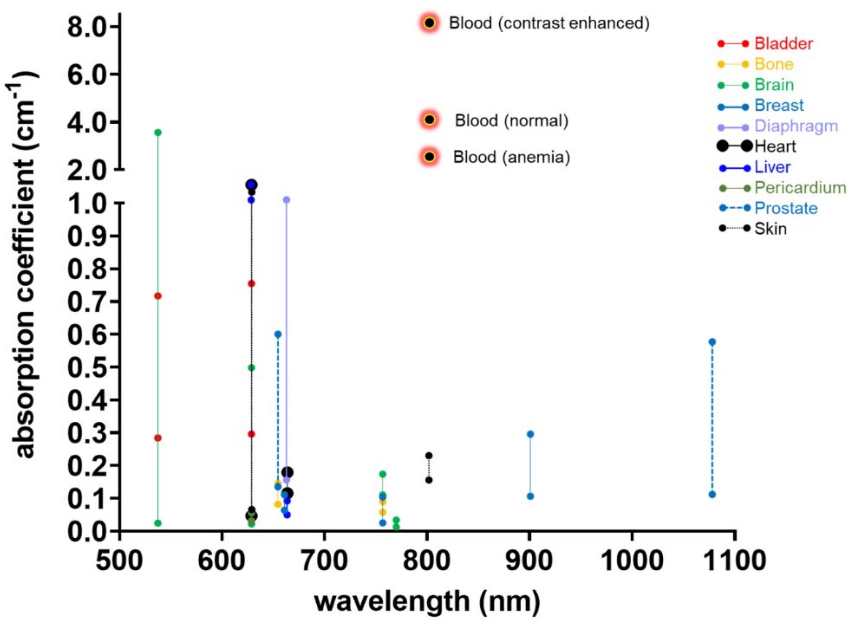

Figure S5. Plot showing the absorption coefficient ranges of different tissue types [1-4].

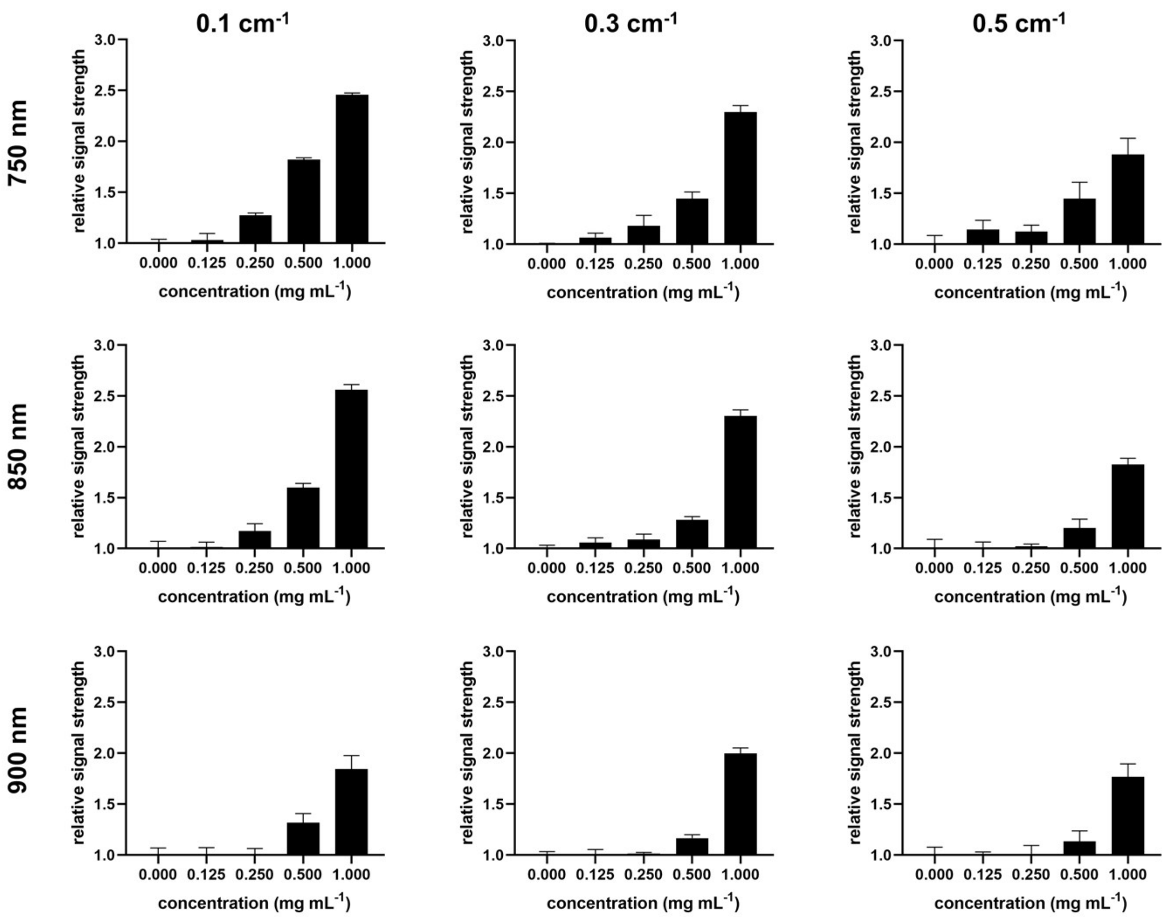

Figure S6. Plots showing the photoacoustic intensity amplification in different tissue-mimicking phantoms by PNE nanobowls, relative to the blood-mimicking phantom (μ_a = 4.0 cm^{-1}) at different photoacoustic imaging wavelengths. All tissue-mimicking phantoms have similar Intralipid® concentration (μ'_s = 13–14 cm^{-1}) with different absorption coefficients of 0.1, 0.3, and 0.5 cm^{-1}.

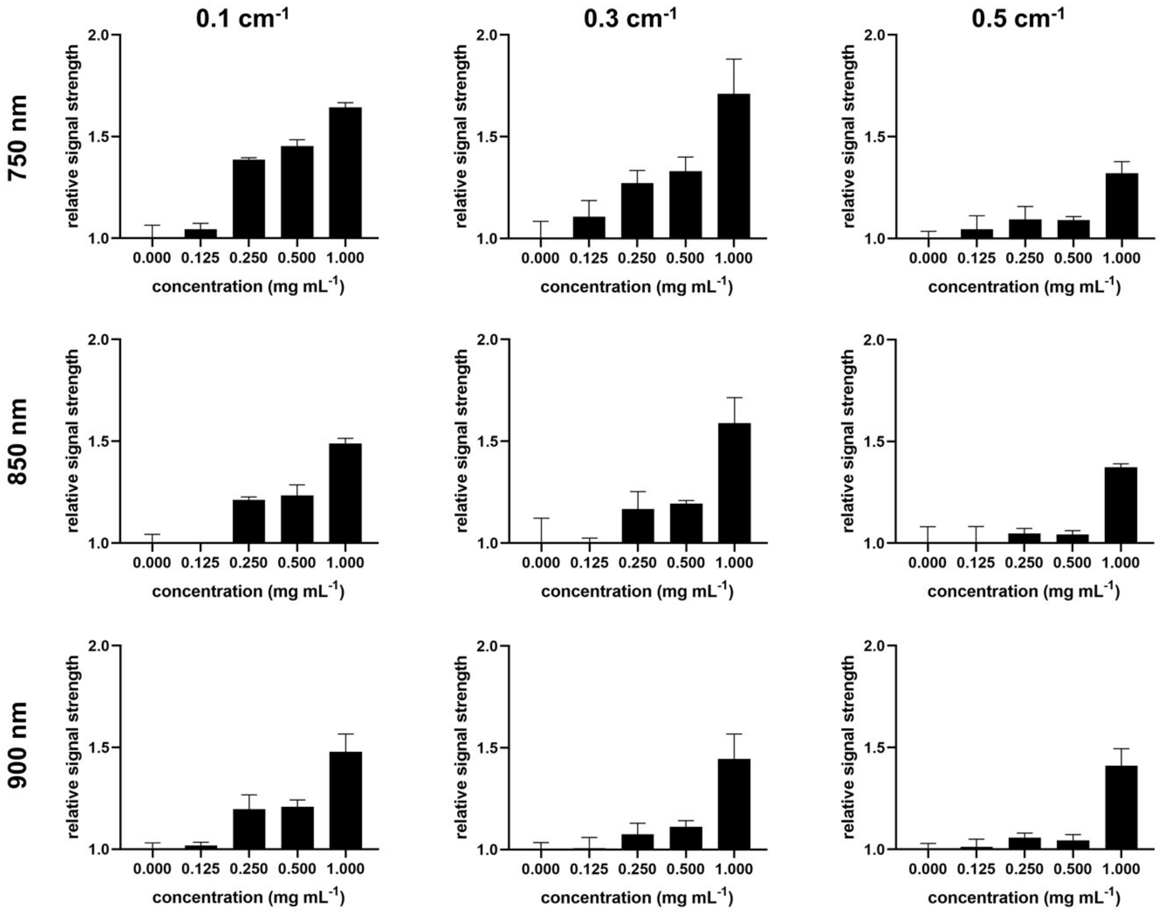

Figure S7. Plots showing the photoacoustic intensity amplification in different tissue-mimicking phantoms by PNE nanospheres, relative to the blood-mimicking phantom (μ_a = 4.0 cm^{-1}) at different photoacoustic imaging wavelengths. All tissue-mimicking phantoms have similar Intralipid® concentration (μ'_s = 13–14 cm^{-1}) with different absorption coefficients of 0.1, 0.3, and 0.5 cm^{-1}.

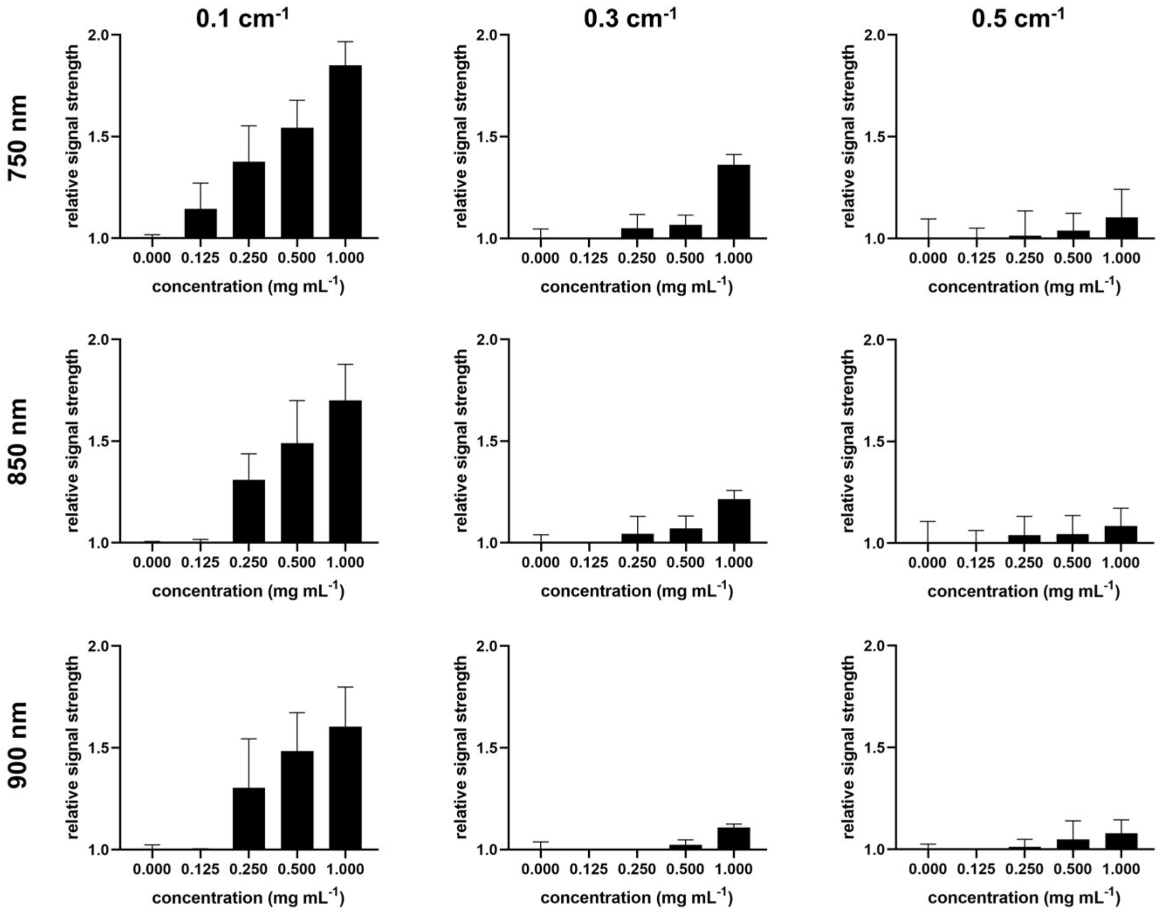

Figure S8. Plots showing the photoacoustic intensity amplification in different tissue-mimicking phantoms by PEP nano-golf balls, relative to the blood-mimicking phantom (μ_a = 4.0 cm^{-1}) at different photoacoustic imaging wavelengths. All tissue-mimicking phantoms have similar Intralipid® concentration (μ'_s = 13–14 cm^{-1}) with different absorption coefficients of 0.1, 0.3, and 0.5 cm^{-1}.

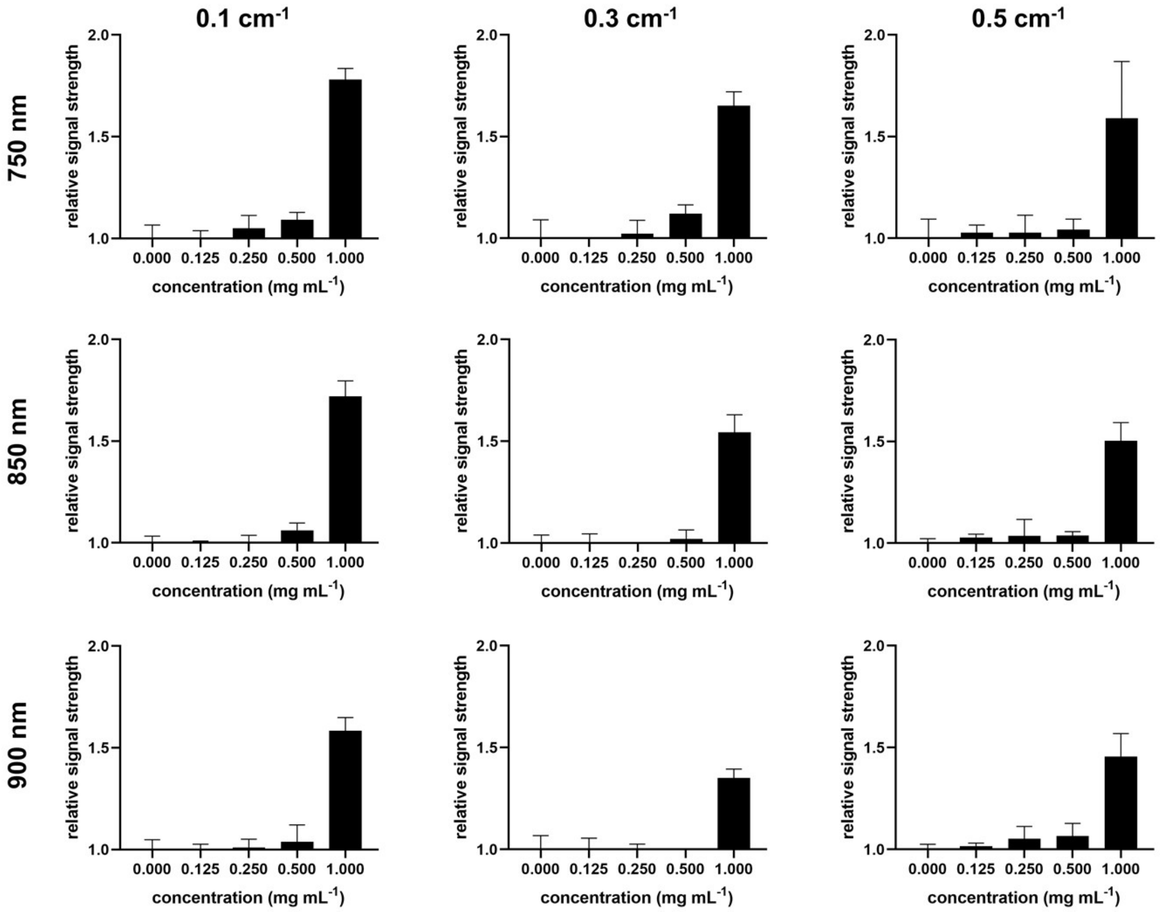

Figure S9. Plots showing the photoacoustic intensity amplification in different tissue-mimicking phantoms by PEP nanospheres, relative to the blood-mimicking phantom (μ_a = 4.0 cm^{-1}) at different photoacoustic imaging wavelengths. All tissue-mimicking phantoms have similar Intralipid® concentration (μ'_s = 13–14 cm^{-1}) with different absorption coefficients of 0.1, 0.3, and 0.5 cm^{-1}.

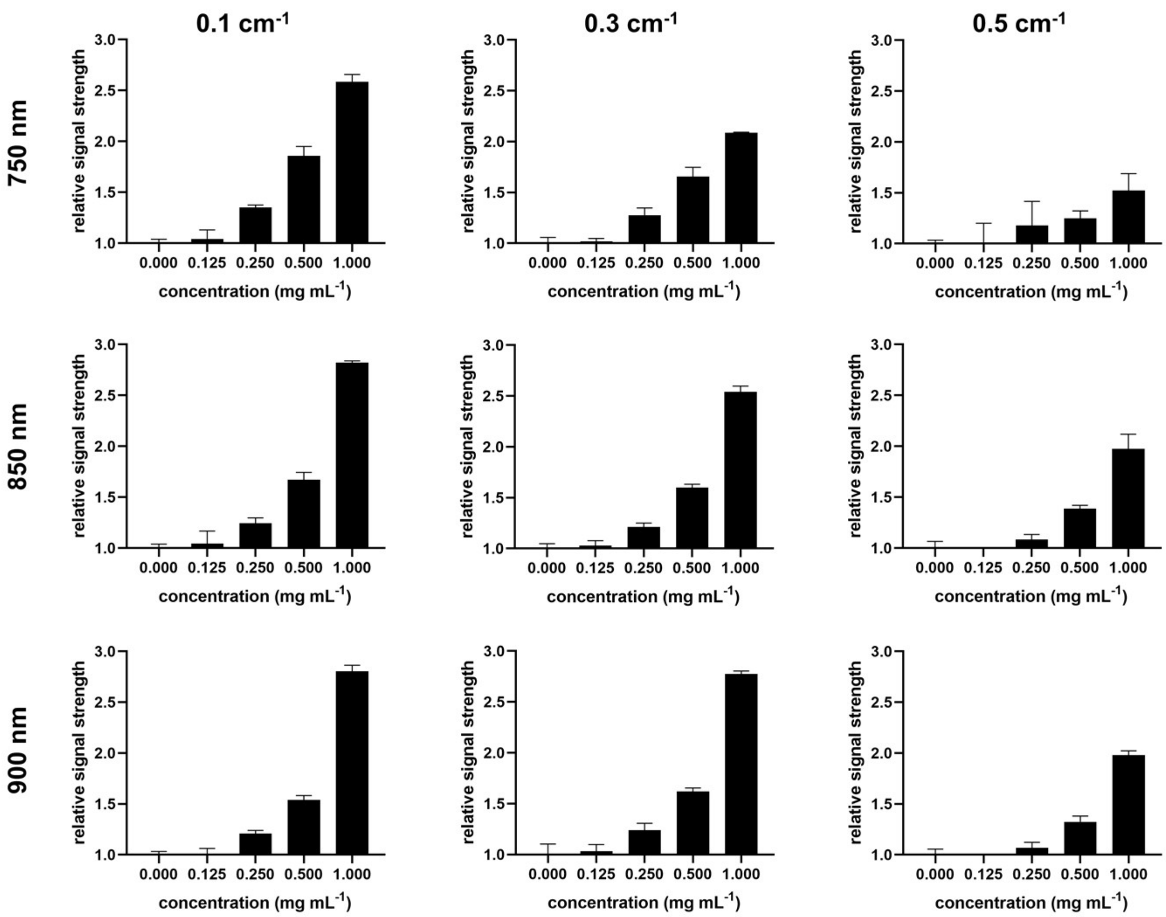

Figure S10. Plots showing the photoacoustic intensity amplification in different tissue-mimicking phantoms by PDA nanobowls, relative to the blood-mimicking phantom (μ_a = 4.0 cm^{-1}) at different photoacoustic imaging wavelengths. All tissue-mimicking phantoms have similar Intralipid® concentration (μ'_s = 13–14 cm^{-1}) with different absorption coefficients of 0.1, 0.3, and 0.5 cm^{-1}.

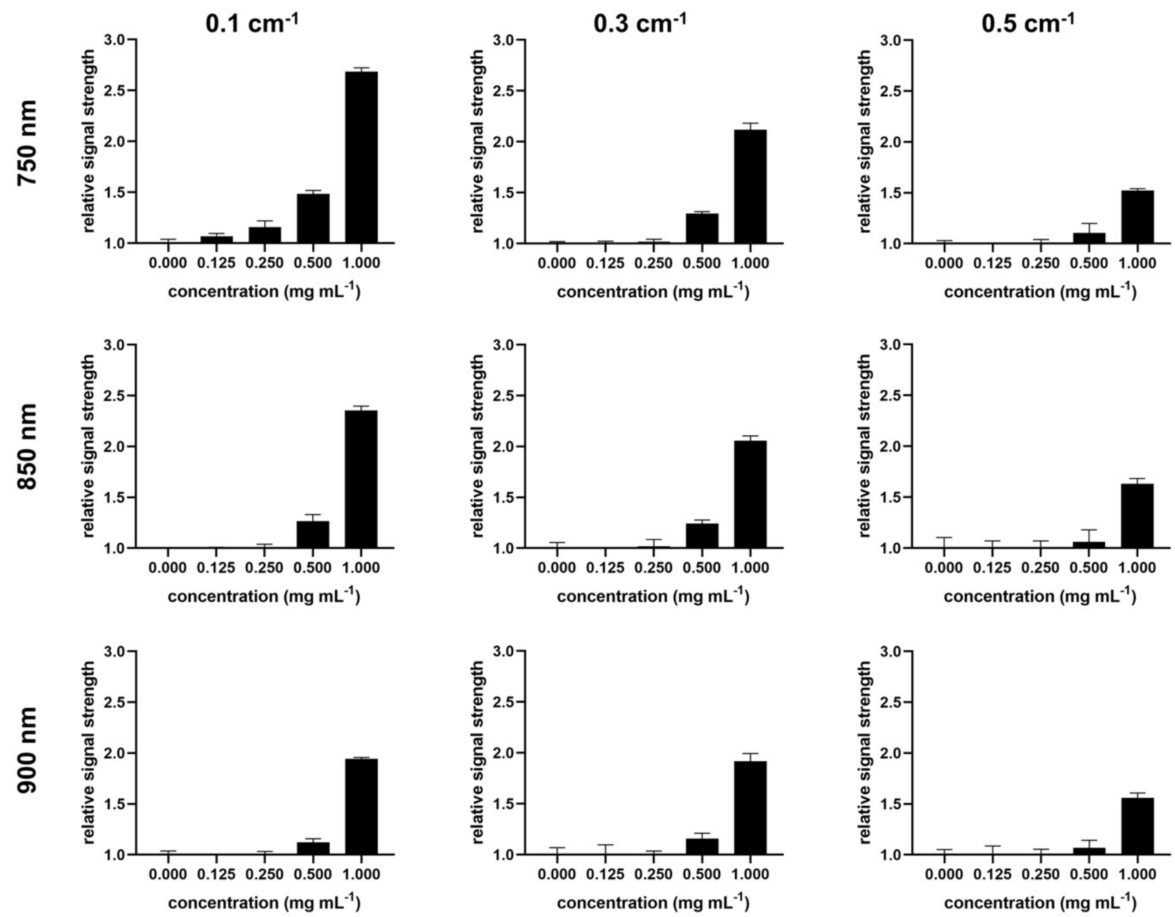

Figure S11. Plots showing the photoacoustic intensity amplification in different tissue-mimicking phantoms by PDA nanospheres, relative to the blood-mimicking phantom (μ_a = 4.0 cm^{-1}) at different photoacoustic imaging wavelengths. All tissue-mimicking phantoms have similar Intralipid® concentration (μ'_s = 13–14 cm^{-1}) with different absorption coefficients of 0.1, 0.3, and 0.5 cm^{-1}.

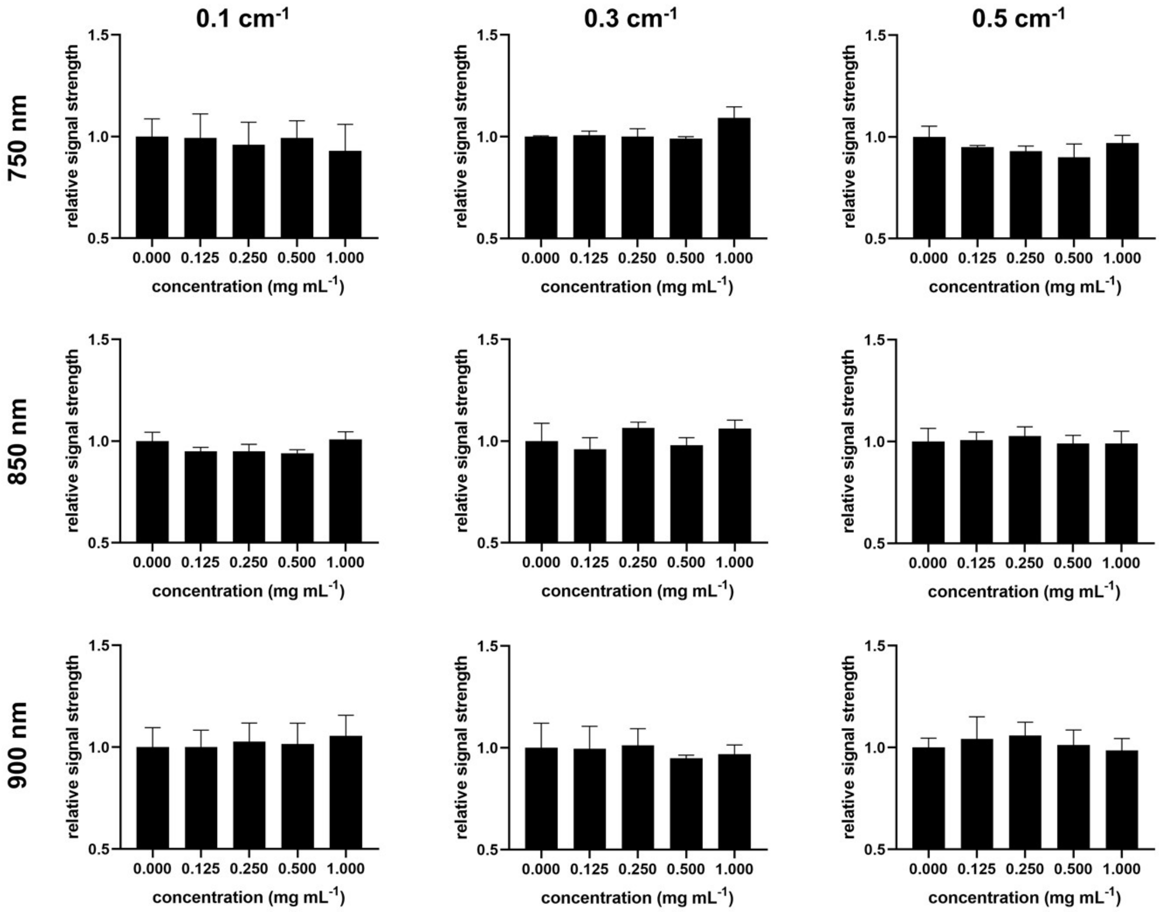

Figure S12. Plots showing the photoacoustic intensity amplification in different tissue-mimicking phantoms by PNE nanoaggregates, relative to the blood-mimicking phantom (μ_a = 4.0 cm^{-1}) at different photoacoustic imaging wavelengths. All tissue-mimicking phantoms have similar Intralipid® concentration (μ'_s = 13–14 cm^{-1}) with different absorption coefficients of 0.1, 0.3, and 0.5 cm^{-1}.

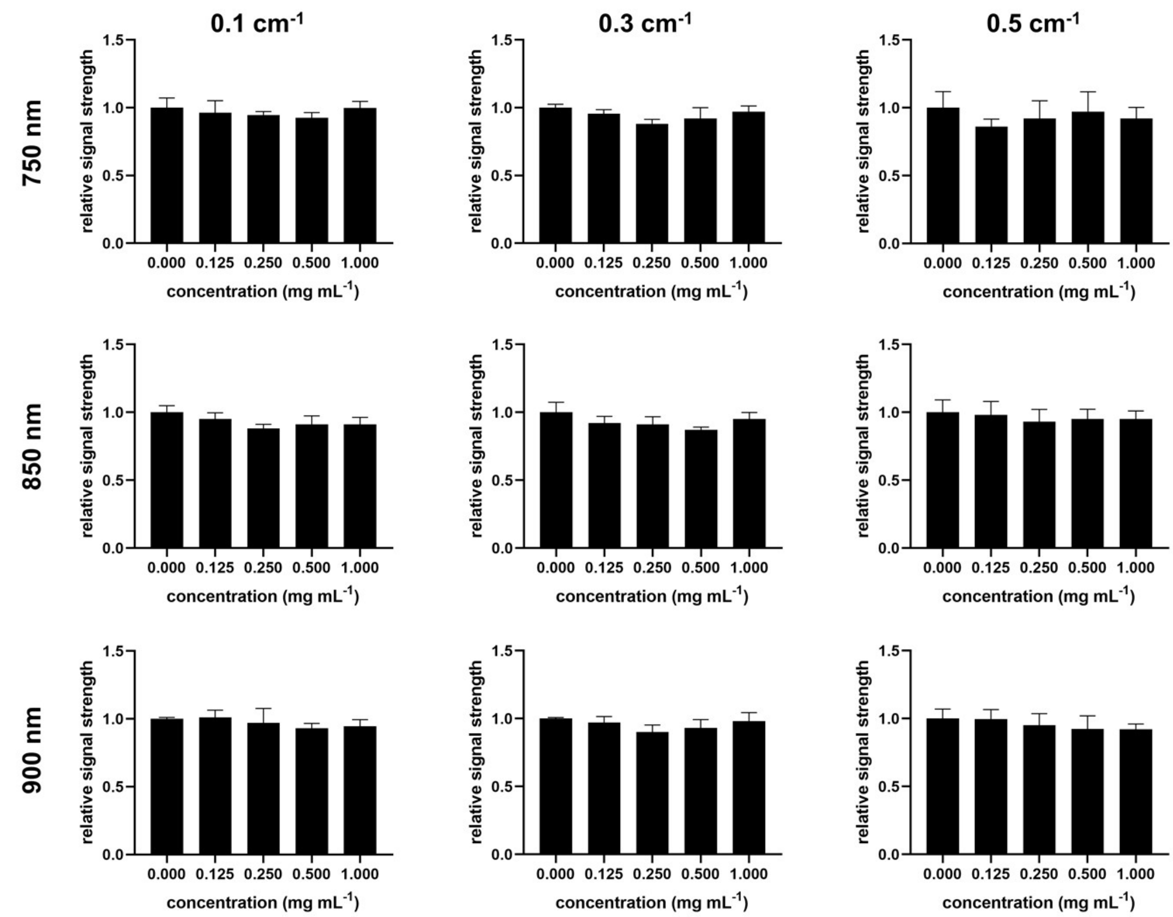

Figure S13. Plots showing the photoacoustic intensity amplification in different tissue-mimicking phantoms by PEP nanoaggregates, relative to the blood-mimicking phantom (μ_a = 4.0 cm^{-1}) at different photoacoustic imaging wavelengths. All tissue-mimicking phantoms have similar Intralipid® concentration (μ'_s = 13–14 cm^{-1}) with different absorption coefficients of 0.1, 0.3, and 0.5 cm^{-1}.

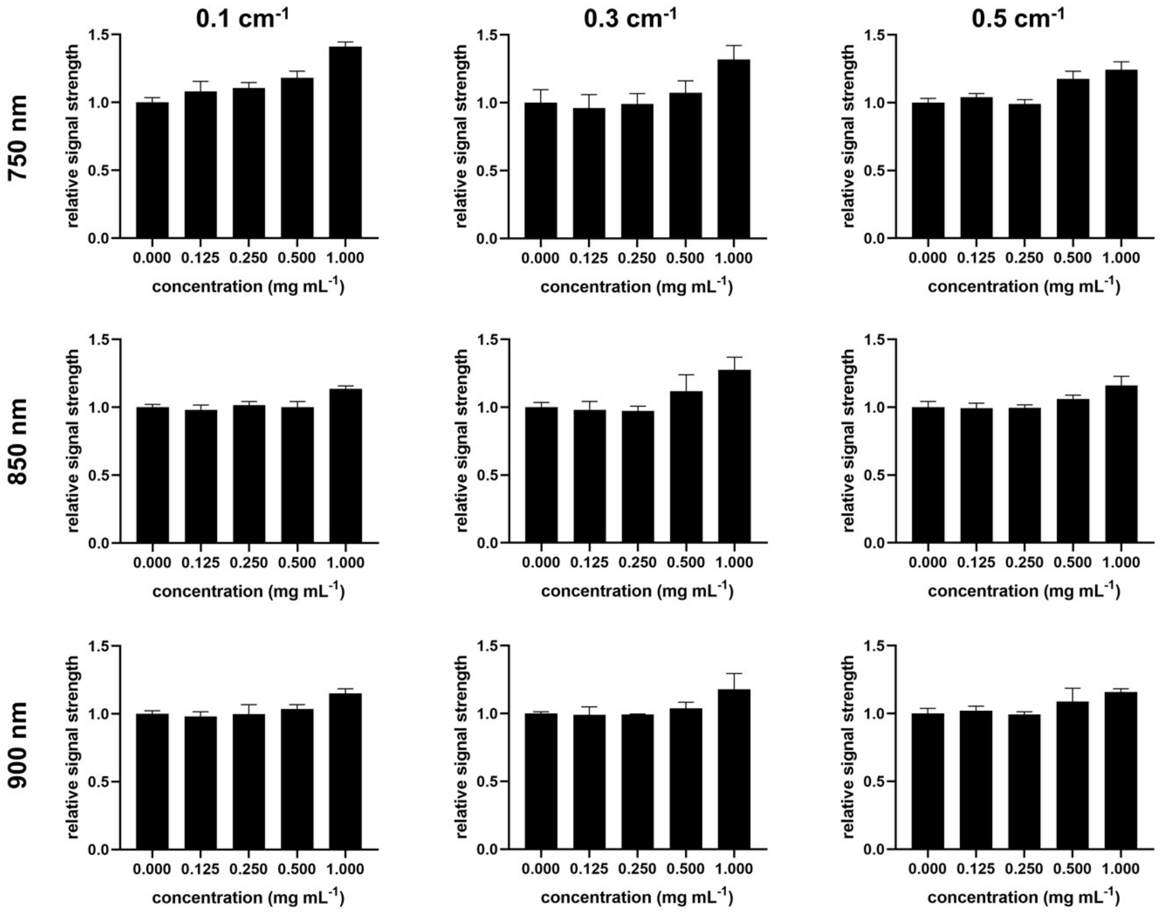

Figure S14. Plots showing the photoacoustic intensity amplification in different tissue-mimicking phantoms by PDA nanoaggregates, relative to the blood-mimicking phantom (μ_a = 4.0 cm^{-1}) at different photoacoustic imaging wavelengths. All tissue-mimicking phantoms have similar Intralipid® concentration (μ'_s = 13–14 cm^{-1}) with different absorption coefficients of 0.1, 0.3, and 0.5 cm^{-1}.

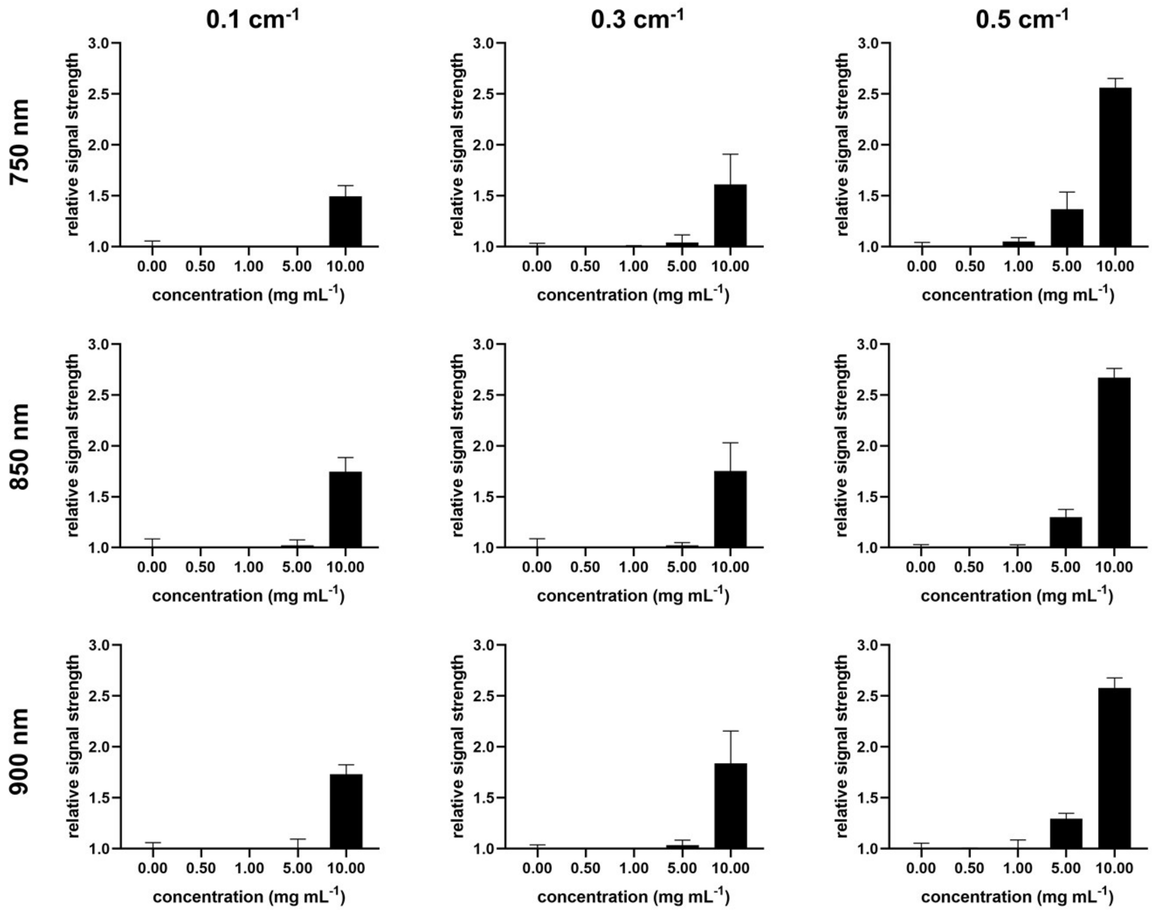

Figure S15. Plots showing the photoacoustic intensity amplification in different tissue-mimicking phantoms by methylene blue, relative to the blood-mimicking phantom (μ_a = 4.0 cm^{-1}) at different photoacoustic imaging wavelengths. All tissue-mimicking phantoms have similar Intralipid® concentration (μ'_s = 13–14 cm^{-1}) with different absorption coefficients of 0.1, 0.3, and 0.5 cm^{-1}.

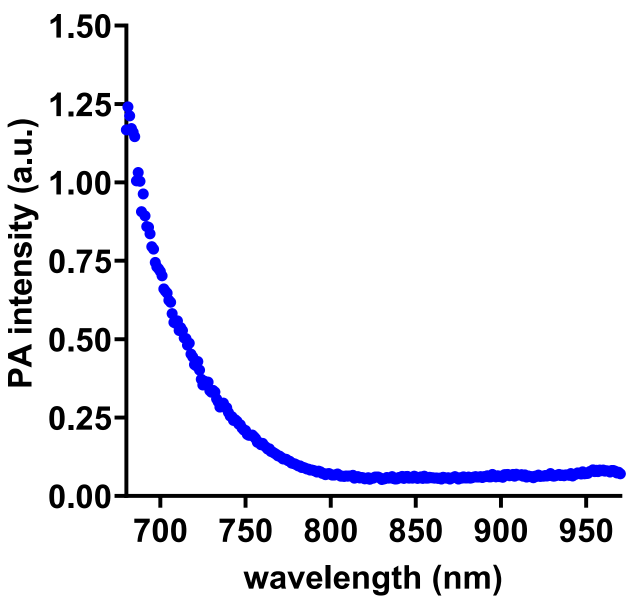

Figure S16. Photoacoustic spectrum of methylene blue.

References

[1] S.L. Jacques, Optical properties of biological tissues: a review, Physics in Medicine and Biology, 58 (2013) R37-R61.
[2] A. Hariri, J. Palma-Chavez, K.A. Wear, T.J. Pfefer, J.V. Jokerst, W.C. Vogt, Polyacrylamide hydrogel phantoms for performance evaluation of multispectral photoacoustic imaging systems, Photoacoustics, 22 (2021) 100245.
[3] H. Lu, F. Floris, M. Rensing, S. Andersson-Engels, Fluorescence Spectroscopy Study of Protoporphyrin IX in Optical Tissue Simulating Liquid Phantoms, Materials, 13 (2020) 2105.
[4] J.L. Sandell, T.C. Zhu, A review of in-vivo optical properties of human tissues and its impact on PDT, Journal of Biophotonics, 4 (2011) 773-787.